Interfacially Polymerized Nanofiltration Membranes: Atomic Force Microscopy and Salt Rejection Studies

A. Wahab Mohammad,[1] Nidal Hilal,[2] M. Nizam Abu Seman[1]

[1]*Department of Chemical and Process Engineering, Universiti Kebangsaan Malaysia, 43600 UKM Bangi, Selangor, Malaysia*
[2]*Centre for Clean Water Technologies, School of Chemical, Environmental, and Mining Engineering, University of Nottingham, University Park, Nottingham, NG7 2RD, United Kingdom*

Received 21 January 2004; revised 28 June 2004; accepted 28 June 2004
DOI 10.1002/app.21157
Published online in Wiley InterScience (www.interscience.wiley.com).

ABSTRACT: Interfacial polymerization is one of the main techniques for producing composite nanofiltration (NF) membranes. In this study, five NF membranes were produced through interfacial polymerization under different conditions of reactions, namely varying reaction time, as well as monomer concentrations. The membranes were then imaged using atomic force microscope (AFM). AFM images provided information of the average pore size, pore size distribution, and surface roughness. For some of the membranes, discrete pore sizes were visible. Increasing the reaction time resulted in decreasing water permeabilities but based on AFM imaging the pore size was of similar value. Increasing the monomer concentration also resulted in decreasing water permeabilities. However, based on AFM imaging the pore size differs considerably. Additional permeation experiments were also carried out using NaCl and Na_2SO_4 solutions with membranes identified as NF. By fitting the rejection data using a model such as the Donnan-steric-pore model, the variation in effective charge density of the membranes was also determined. The ability to tailor composite NF membranes with the right properties will significantly improve membrane performance. © 2005 Wiley Periodicals, Inc. J Appl Polym Sci 96: 605–612, 2005

Key words: atomic force microscopy (AFM); membranes; modeling

INTRODUCTION

Nanofiltration (NF) membranes have been recognized for having properties in between those of ultrafiltration and reverse osmosis and thus have found applications in many areas, especially in rejecting ions and charged organic pollutants. Due to the charged (mostly negative) nature of the membranes, the separation performance is influenced not only by the steric effect, but also by the charge or Donnan effect.

One of the main techniques to produce NF membranes is through the interfacial polymerization technique. The technique has been used to produce commercially successful NF membranes such as the NF-45 membrane by Dow.[1] Membranes produced using this technique are considered thin film composite membranes due to the thin layer deposited on top of the support structure. The thin layer allows for higher flux to be obtained while maintaining similar rejection properties compared to asymmetric membranes. Various studies have been carried out to observe the effect of several parameters involved during the interfacial polymerization process.[2,3] Most of the studies, however, depended on solute rejection results to ascertain the effect of certain parameters on the characteristics of the membranes produced.

For NF membranes, a microscopy technique such as scanning electron microscopy is not suitable due to the nanoscale dimension involved. An alternative technique would be to use atomic force microscopy (AFM) to study the surface morphology of these membranes. AFM[4] is a relatively newly developed technique that gives topographic images by scanning a sharp tip over a surface[5] and has been used to produce atomic resolution images of both conductors and nonconductors.[6] AFM can image both conductive and nonconducting surfaces with nanometre scale resolution in air and even under liquids. Consequently, the samples need not be exposed to vacuum, and preparation techniques like evaporating a thin metal coating or taking a replica are unnecessary. Even soft organic surfaces can be successfully imaged with AFM because the use of microfabricated cantilevers[6] allows operation with total forces between 10^{-7} and 10^{-8} N in contact mode and in the order of 10^{-12} N in noncontact mode.

The study of the surface morphology of membranes can help one to understand the separation processes in these membranes as the characteristics of pore struc-

Correspondence to: A. W. Mohammad (wahabm@vlsi.eng.ukm.my).

Contract grant sponsor: Malaysian Ministry of Science, Technology & Environment; contract grant number: IRPA 09-02-02-0067.

ture (pore diameter, pore density, and pore size distribution) determine their filtration properties. However, a high-resolution microscope is necessary to observe the small pores, especially in nanofiltration membranes.[7–9] Our previous studies concerning the use of AFM[7,10] on NF membranes showed that discrete pores with measurable dimension can be well observed.

In trying to model the performance of NF membranes, the membranes are typically characterized in terms of the effective pore radius, r_p, (accounting for steric effect), and effective charge density, X_d, (for the Donnan effect).[11–13] An additional parameter would normally be the effective ratio of membrane thickness over porosity, $\Delta x/A_k$. Once these parameters are obtained, it is possible to use models such as those based on the extended Nernst–Planck equation to simulate the separation performance of the membranes.[14]

Previously we showed[15] that the commercially available NF membranes have wide ranging characteristics of r_p, $\Delta x/A_k$, and X_d. In subsequent work,[16] it was shown that selection of suitable membrane characteristics for specific processes will allow for higher efficiency and improvements in the process. Therefore, there is the so-called "optimized" membrane parameters, which, if it were to be used, would certainly help in reducing the cost of membrane applications in the industry. The ability to produce nanofiltration membranes with optimized properties will certainly provide significant improvement in terms of membrane performance and processing cost reduction.[17] Thus, by understanding the variation of properties during the interfacial polymerization process, it would lead toward better NF membranes for future applications.

The main objective of this paper then is to use information from atomic force microscopy to understand the characteristics of NF membranes produced using the interfacial polymerization technique. AFM was used to study the membrane properties providing data on pore size, pore size distribution, and surface roughness. Additional permeation experiments were also conducted with water, NaCl, and Na_2SO_4. For the salt rejection data, additional interpretation by fitting the data to model such as the Donnan–steric–pore model[7] was required in order to obtain an estimate of the effective charge density. By this mean, the trend of variations of r_p, $\Delta x/A_k$, and X_d of the membranes can be determined.

MATERIALS AND METHOD

Six membranes were fabricated using the interfacial polymerization technique. The membrane support was made from a mixture of polysulfone (P1835-BP Amoco) and polyvinylpyrrolidone (Fluka) with *N*-methyl-2-pyrrolidinone as the solvent. The top active layer was obtained through interfacial polymerization between trimesoyl chloride (Aldrich) in hexane (Merck) with aqueous phase containing bisphenol A (BPA) (Aldrich). BPA acted as the monomer for the interfacial polymerization reaction. Table 1 shows the summary of the membrane preparations. The first three membranes identified as PT-30, PT-45, and PT-60 differ in their dipping time during the interfacial reaction. The other three membranes identified as PC-05, PC-1, and PC-2 differ in terms of the concentration of BPA used during the interfacial polymerization. PT-45 is essentially equivalent to PC-1 membrane.

TABLE 1
Summary of Membranes Fabricated

Membranes	Reaction time (s)	BPA concentration (wt %)
PT-30	30	1
PT-45	45	1
PT-60	60	1
PC-05	45	0.5
PC-1	45	1.0
PC-2	45	2.0

AFM imaging

AFM was used to vizualize the surface structures of membranes. The AFM used in this study was an Explorer (TMX 2000), a commercial device from Vecco Instruments. High-magnification images of membrane surfaces can be obtained with the use of microfabricated cantilevers.[19] A silicon cantilever (Ultralevers, Park Scientific Instruments) with a high aspect ratio tip of typical radius of curvature 5–10 nm was used to scan the membrane and produce the images. The profile imaging mode was selected to study the polymeric membranes at room temperature of 25°C. This imaging mode has not been previously used for imaging membrane surfaces; it has many advantages over other AFM modes. In the profile imaging mode, the image was acquired by having the tip approach the surface at a speed of 300 μm/s. At such speed the feedback signal was more positive than the set point, -5 nA. The Z level was recorded as topographic information. The tip was retracted above the sample by a fixed distance (Z pullout of 3100 nm) and the tip was moved laterally to the next position at the top of the pullout cycle. The process was repeated at each data point to establish the topographic profile of the membrane surface. The images were obtained over an area of 30×30 μm for both initial and modified membranes. Membrane surface parameters such as the root mean square of Z values and total contact area can be obtained from the images.

TABLE II
Equations for the DSPM Model

Equations for the Donnan–steric–pore (DSPM) model

Main equations

Concentration gradient

$$\frac{dc_i}{dx} = \frac{J_v}{D_{i,p}}(K_{i,c}c_i - C_{i,p}) - \frac{z_i c_i}{RT} F \frac{d\psi_m}{dx} \quad (a)$$

Potential gradient

$$\frac{d\psi_m}{dx} = \frac{\sum_{i=1}^{n} \frac{z_i J_v}{D_{i,p}}(K_{i,c}c_i - C_{i,p})}{\frac{F}{RT}\sum_{i=1}^{n}(z_i^2 c_i)} \quad (b)$$

where:

Donnan–steric partitioning

$$\left(\frac{\gamma_i c_i}{\gamma_i^0 C_i}\right) = \Phi \exp\left(-\frac{z_i F}{RT}\Delta\psi_D\right) \quad (c)$$

Hindrance factors

$$K_{i,d} = K^{-1}(\lambda,0) \quad K_{i,c} = (2-\Phi)G(\lambda,0) \quad (d)$$

$$D_{i,p} = K_{i,d} D_{i,\infty} \quad (e)$$

Hydrodynamic drag coefficients

$$K^{-1}(\lambda,0) = 1.0 - 2.30\lambda + 1.154\lambda^2 + 0.224\lambda^3 \quad (f)$$

$$G(\lambda,0) = 1.0 + 0.054\lambda - 0.988\lambda^2 + 0.441\lambda^3 \quad (g)$$

Steric partitioning

$$\Phi = (1-\lambda)^2 \quad (h)$$

Electroneutrality conditions

$$\sum_{i=1}^{n} z_i C_i = 0 \quad \sum_{i=1}^{n} z_i c_i = -X_d \quad (i)$$

Permeation experiment

Permeation experiments were carried out with distilled water, NaCl, and Na_2SO_4 solutions. The NaCl and Na_2SO_4 used were of high purity grade and were obtained from Fluka. Solutions were prepared with distilled water. The membranes were immersed at least overnight in such water before being used in any experimental work. All solutions were thermostated at 25 ± 0.2°C in a water bath for at least 1 h before being used in the experiment. The salt concentrations were measured using a conductivity meter (Inolab).

A stirred Amicon ultrafiltration cell, Model 8200, was used in the experiments. It had a volume capacity of 200 ml and could hold a membrane disc 62 mm in diameter. The effective area of the membrane was 28.7 cm^2. The maximum operating pressure of the cell was 517 kN m^{-2} (75 psia). This limited operating pressure thus restricted the range of fluxes that can be investigated. Therefore, for the permeation experiments only three applied pressure were used, namely 25.0, 45.0, and 65.0 psia.

Donnan–steric–pore model (DSPM)

The rejection data of NaCl at various concentrations were fitted to the Donnan–steric–pore model in order to determine the variation of effective charge density, X_d, of the membranes. DSPM was used previously to describe the transport of ions/solutes inside the membranes.[7,10] The extended Nernst–Planck equation forms the basis for the model and can be written as

$$j_i = -D_{i,p}\frac{dc_i}{dx} - \frac{z_i c_i D_{i,p}}{RT} F \frac{d\psi}{dx} + K_{i,c} c_i V, \quad (1)$$

where j_i is the flux of ion i and the terms on the right-hand side represent transport due to diffusion,

TABLE III
Characteristics of the Membranes

Membrane	Water permeability (L m^{-2} h^{-1})	r_p^s using AFM (nm)	$\Delta x/A_k$ (μm)	k'	n
PT-30	34.53	1.68	3.87	26.85	0.654
PT-45[a]	14.78	1.57	7.85	22.26	0.632
PT-60	9.97	1.21	6.96	6.95	0.620
PC-05	37.78	5.36	36.02	Not analyzed	
PC-1[a]	14.87	1.57	7.85		
PC-2	2.60	<0.4	2.92		

[a] The same membrane.

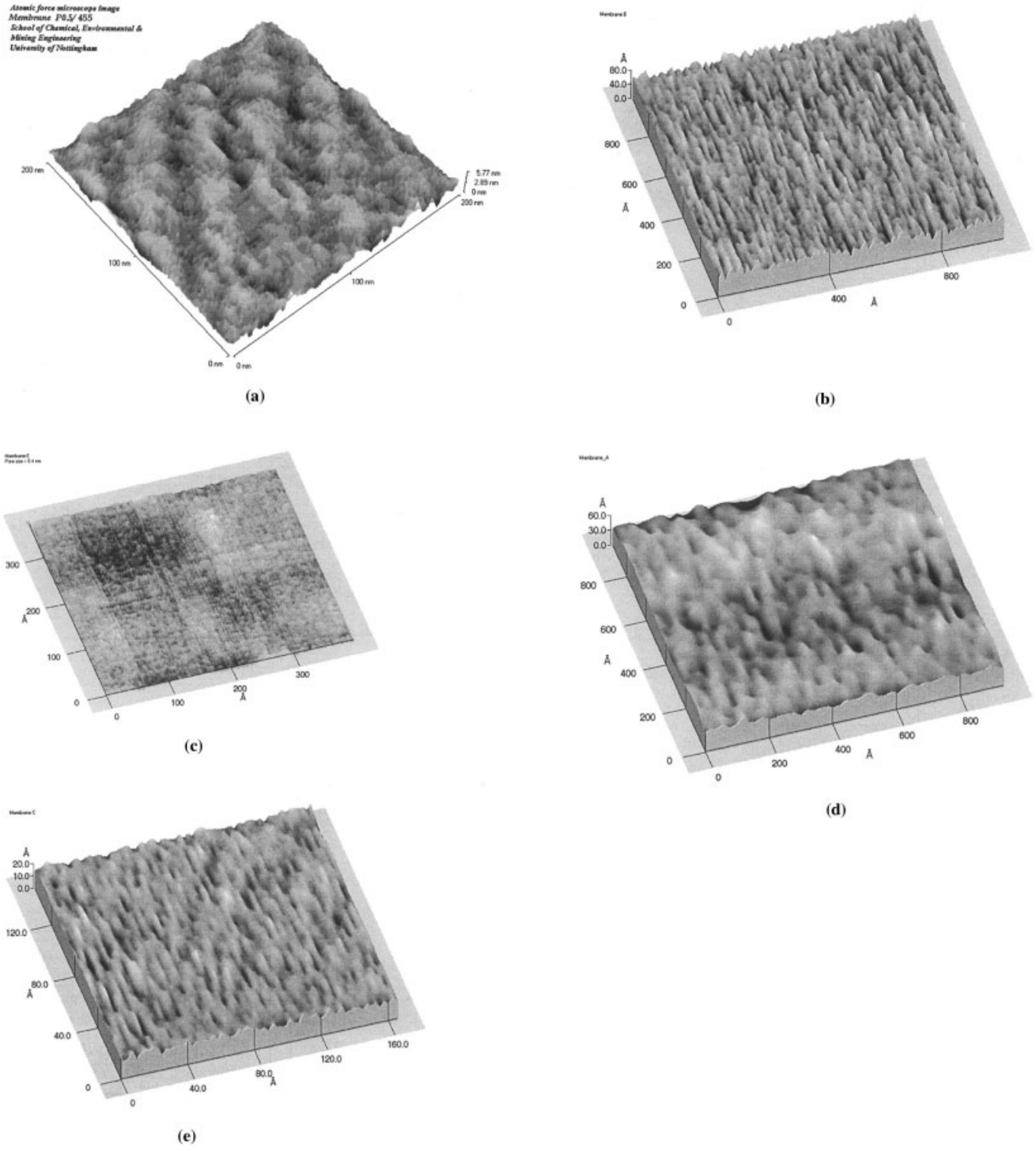

Figure 1 AFM surface images of various membranes: (a) PC-05, (b) PC-1/PT-45, (c) PC-2, (d) PT-30, and (e) PT-60.

electric field gradient, and convection, respectively. The hindered nature of diffusion and convection of the ions inside the membrane are accounted for by the terms $K_{i,\mathrm{d}}$ and $K_{i,\mathrm{c}}$. Further details for solution of this equation for transport through NF membranes can be found elsewhere.[7,14,15] Table 2 shows other supporting equations used in this model.

The DSPM model depends on three NF membrane parameters: effective pore radius, r_{p}, effective charge density, X_{d}, and effective ratio of membrane thickness to porosity, $\Delta x/A_{\mathrm{k}}$. The r_{p} was obtained from the AFM measurement while $\Delta x/A_{\mathrm{k}}$ was obtained from the Hagen–Poiseuille relationship between water flux and applied pressure, as shown below,

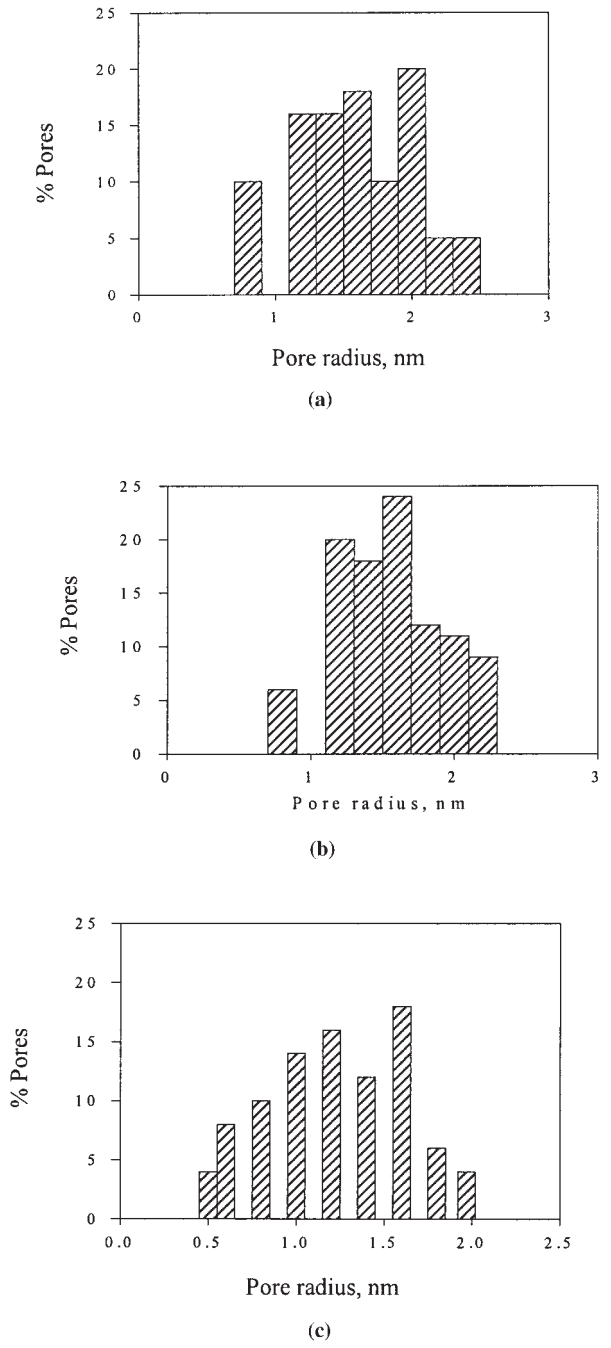

Figure 2 Pore size distribution of membranes: (a) PT-30, (b) PT-45, and (c) PT-60.

$$J_w = \frac{r_p^2 \Delta P}{8\mu(\Delta x/A_k)}, \quad (2)$$

where J_w is permeate flux, μ is the viscosity, ΔP is the applied pressure.

An estimate of the charge density variation of the membranes can be obtained by fitting the rejection data of NaCl to the DSPM model. Based on this charge density, the rejection of Na_2SO_4 can be predicted using the model. Thus, the predicted rejection and experimental rejection of Na_2SO_4 will also be compared.

RESULTS AND DISCUSSION

Water permeation of the membranes

Table 3 shows the summary of the permeation study carried out with distilled water using the six membranes prepared. As shown in the second column of Table 3, the permeability decreased significantly as the reaction time and BPA concentration were increased. The range of values obtained was well within the range of values reported previously for NF membranes available commercially, which is between 1.331 and 50.50 L m^{-2} h^{-1} bar^{-1}.[15]

Reaction time as well as the concentration of BPA affect the water permeability very much. Ji and Mehta[20] reported that the growth of thin film depends very much on the reactant concentration. In this case as the BPA concentration was increased, the thin film composite layer was postulated to be thicker and thus resulted in lower permeabilities. A similar effect is expected as a function of the reaction time. In this case, longer reaction time will induce a thicker thin film layer on top of the polysulfone support.

AFM imaging

It should be noted that the pore dimension obtained using AFM is not exact due to the uncertainty in absolute dimension measurements caused by convolution of the AFM tip and pore shapes at the nanometer scale.[10] However, for the purpose of this study, the results from AFM can be used for relative comparison of the pore dimensions of the six membranes as well as to determine the pore size distribution of the membranes.

The AFM was used to image the surface of each of the membranes. Figure 1a–e shows the surface image of membranes PC-05, PC-1/PT-45, PC-2, PT-30, and PT-60, respectively. The images clearly show the existence of discrete pores in the membranes except for the PC-2 membrane. Table 3 lists the pore size of all membranes. It can be seen that for the PT-30, PT-45, and PT-60 membranes, the pore size did not vary much. In this case, the variation of reaction time affected the flux very much but not the effective pore sizes. How-

TABLE IV
Root Mean Square Roughness Value (RMS) for All Membranes

Membrane	RMS (nm)
PT-30	0.4857
PT-45	0.4627
PT-60	0.5859

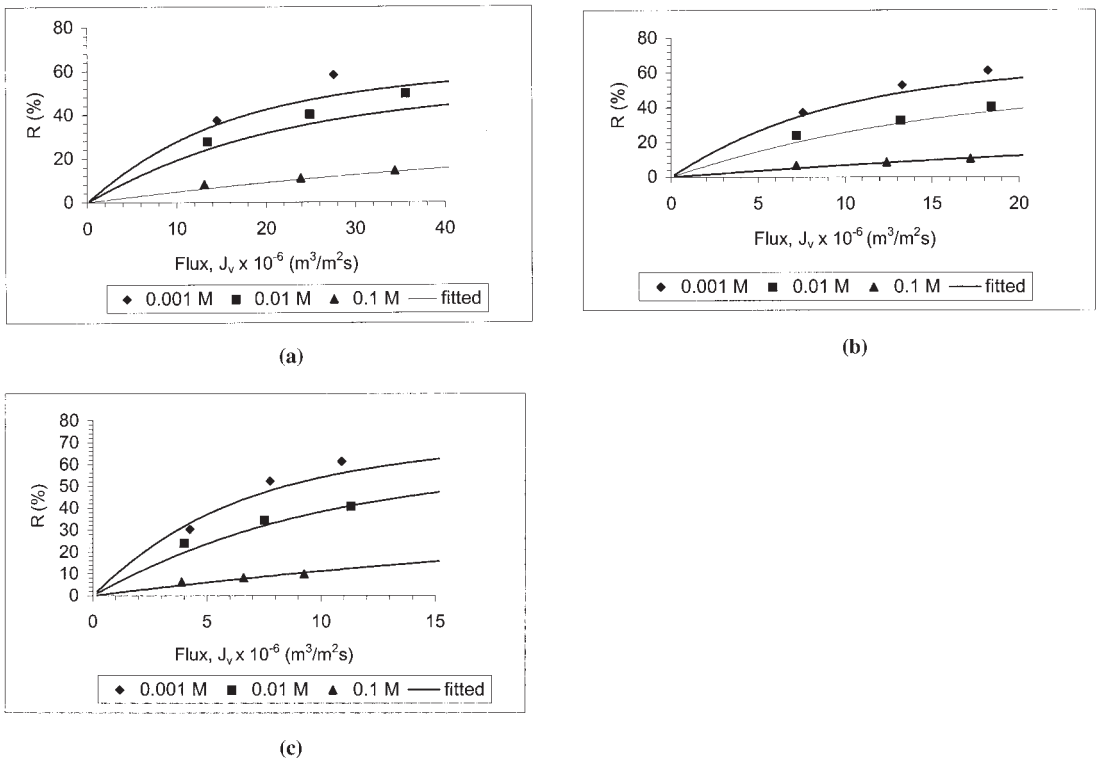

Figure 3 Experimental and fitted data for NaCl rejections vs permeate fluxes: (a) PT-30, (b) PT-45, and (c) PT-60.

ever, for membranes PC-05, PC-1, and PC-2, the pore sizes vary significantly. For PC-05, the large pore size was not expected and in this case the PC-05 membrane was possibly closer to the ultrafiltration membrane. PC-2 membranes meanwhile may be considered reverse osmosis membranes since the pores were not visible (<0.4 nm). Thus, for subsequent detailed studies, only the three membranes (PT-30, PT-45, and PT-60) were considered since they represent NF structural properties.

The pore size distribution was determined for the three membranes. Figure 2 shows the pore size distribution of the three membranes. It can be seen that the pore size distribution was quite wide, indicating the typical distribution of polymeric membranes. Further measurement of the root mean square roughness value (RMS) of the three membranes was also made. Table 4 shows the RMS values for the three membranes, PT-30, PT-45, and PT-60. The software of the AFM allows quantitative determination root mean square of Z values as the square root of the mean value of the triangles of the distance of the point from the image mean value over each data point:

$$\text{RMS} = \sqrt{\frac{1}{N}\sum_{i=1}^{N}\langle Z_i - Z\rangle^2}, \tag{3}$$

where Z_i is the current Z value, while Z and N are the average of Z values and the number of points within the area, respectively.

Average height gives the arithmetic mean defined as

$$|Z| = \frac{1}{N}\sum_{i=1}^{N} Z_i. \tag{4}$$

Total contact surface area is calculated including the height (Z data; Z_1, Z_2, Z_3, and Z_4) of every four adjacent pixels. The surface of the square described as Z_1, Z_2, Z_3, and Z_4 is computed by dissecting the square into triangles and then computing the area of each triangle,

$$a = \sqrt{(\Delta x)^2 + (\Delta Z_{12})^2}, \tag{5}$$

where $\Delta Z_{12} = Z_1 - Z_2$,

$$b = \sqrt{(\Delta y)^2 + (\Delta Z_{24})^2}, \tag{6}$$

where $\Delta Z_{24} = Z_2 - Z_4$,

$$c = \sqrt{(\Delta z)^2 + (\Delta Z_{14})^2}, \tag{7}$$

where $\Delta Z_{14} = Z_1 - Z_4$.

The surface of a single triangle is then calculated as

$$S = \sqrt{p(p-a)(p-b)(p-c)}, \tag{8}$$

where $p = 12(a+b+c)$.

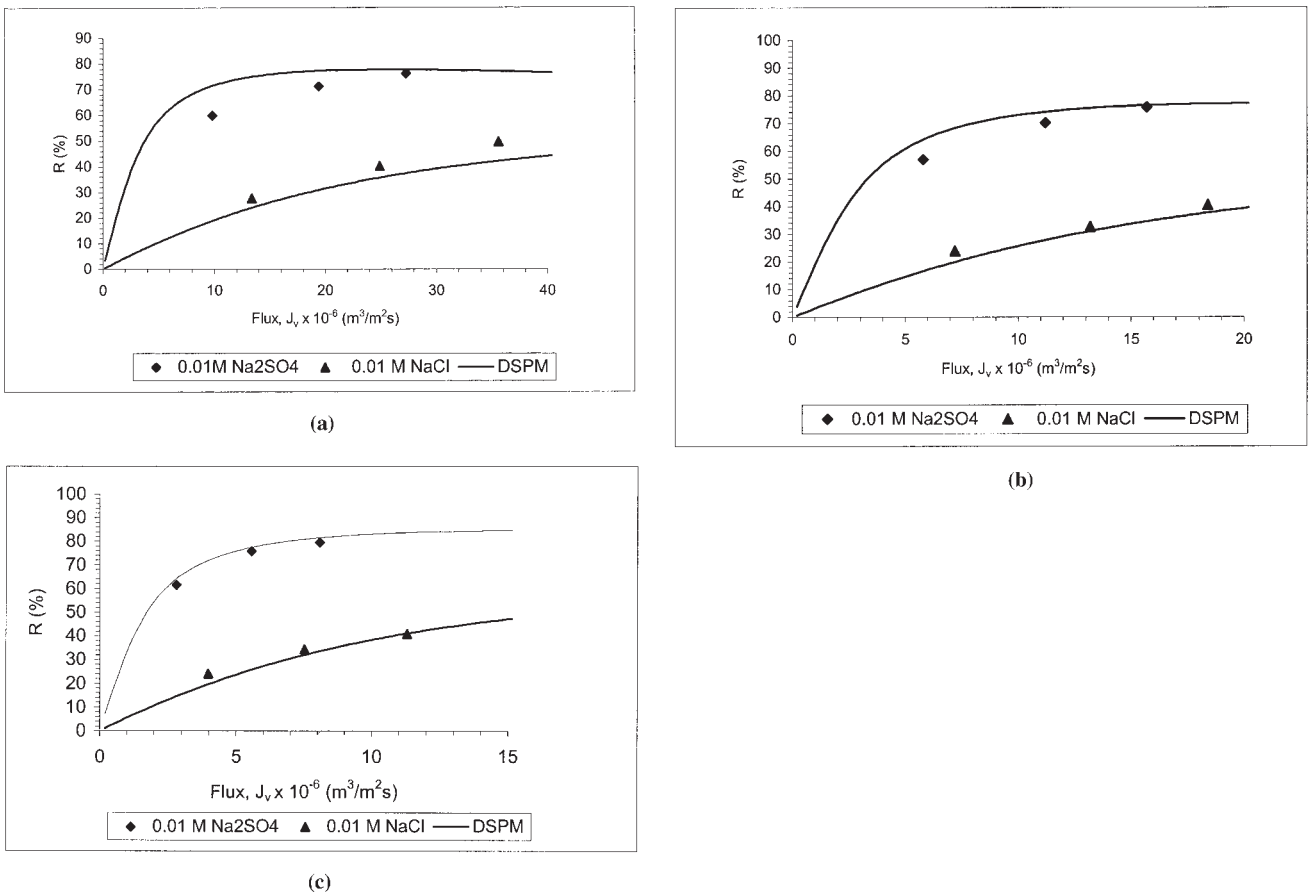

Figure 4 Predicted rejection of Na_2SO_4 based on DSPM compared to the experimental rejection for membranes: (a) PT-30, (b) PT-45, and (c) PT-60.

This calculation was applied to the entire imaged surface in order to get the total surface area including the z variations. So the ratio of the projected area over the surface area gives a good indication of the sample surface area deviation in relation to the geometric flat surface.

It was reported recently[19] that surface roughness had a significant impact on the increase in membrane productivity. Thus, the ability to measure surface roughness and relate it to membrane performance should be investigated in the future. AFM measurement will allow such direct quantification of surface roughness and this can be directly related to the membrane productivity. The three membrane samples measured in this study were inadequate to lead to any conclusions.

Fitting to the DSPM model

Permeation experiments were carried out with 0.001, 0.01, and 0.1 *M* NaCl at applied pressure ranging from 1.5 to 4.5 bar and the result was interpreted using the Donnan–steric–pore model mentioned previously. Again these were done only for the three membranes: PT-30, PT-45, and PT-60. In order to use the DSPM model, three parameters characteristics of the membrane are required, namely effective pore radius, r_p, effective thickness over porosity, $\Delta x/A_k$, and effective charge density, X_d. In this work, r_p would be taken from the average r_p as provided by the AFM image. $\Delta x/A_k$ was then determined from Eq. (2). The membrane thickness for the PT series membranes did not differ by much in the range of 3.92–7.85 μm. For the PC series membranes, $\Delta x/A_k$ decreased as the BPA concentration increased. The variation in the thickness of the thin film is the main reason why the permeate flux decreased for the PT series (effect of r_p about the same), while for the PC series the reduction in permeate flux is caused by mainly by reduction of r_p since the decreasing thickness would have the opposite effect on flux.

The salt rejection data were then fitted with the DSPM model in order to obtain X_d. Figure 3 shows the plots of the fitted rejection data of NaCl at different concentrations for membranes PT-30, PT-45, and PT-60. The fitting with the DSPM model is reasonably good using the parameters obtained from the AFM imaging.

The effective charge density, X_d, can be related to the NaCl concentrations through some type of isotherms. One of the commonly used forms is the following Freundlich isotherm form:[20]

$$X_d = k' C_b^n. \quad (9)$$

The fifth and sixth columns of Table 2 shows the values of k' and n as obtained through the fittings of Eq. (3). The results show that the k' values increased for the PT membranes $k'_{\text{PT-30}} > k'_{\text{PT-45}} > k'_{\text{PT-60}}$. The values of n for all membranes were similar, in the region of 0.62–0.65. Based on the results of this study, it seems that the effective charge density (moles of charge/volume) is higher for a thinner thin film membrane compared to the thicker membrane, which indirectly contributed to the decrease in salt rejection.

The values of r_p, X_d, and $\Delta x/A_k$ were then used to predict the rejection of Na_2SO_4. Our previous study[21] showed that the predictive capability of DSPM was quite remarkable for monovalent cation of salts such as NaCl and Na_2SO_4. In such cases, the rejection of Na_2SO_4 can be predicted based on the X_d obtained from NaCl rejection. X_d should be taken to be a function of the concentration of Na^+ ions. Thus, for 0.01 *M* Na_2SO_4 the concentration, C_b, which should be used in Eq. (7), is 0.02 *M*. Figure 4 shows the predicted rejection of Na_2SO_4 based on DSPM compared to the experimental rejection for membranes PT-30, PT-45, and PT-60. The results shows that the agreement between predicted and experimental rejections was quite good.

CONCLUSIONS

Based on the findings from this study, atomic force microscopy is a useful tool to observe the variations of the NF membrane properties obtained using the interfacial polymerization technique. The variation of reaction time as well as monomer concentrations can affect the properties of the membrane produced. Increasing the reaction time resulted in decreasing water permeabilities, but based on AFM imaging, the pore size was of equal value. Increasing the monomer concentration also resulted in decreasing water permeabilities. However, based on AFM imaging the pore size differs considerably. Additional permeation experiments and data interpretation with predictive model such as the DSPM model allow further understanding of the variation of membrane properties. The effective pore sizes obtained from AFM data were shown to be able to fit the rejection data quite well. Through DSPM model fitting, the effective charge density was also found to be quite varied.

References

1. Petersen, R. J. J Membr Sci 1993, 83, 81.
2. Jayarani, M. M.; Kulkarni, S. S. Desalination, 2000, 130, 17.
3. Lu, X.; Bian, X.; Shi, L. J Membr Sci 2002, 210, 3.
4. Binning, G.; Quate, C. F.; Gerber, Ch. Phys Rev Lett 1986, 56, 930.
5. Hansma, P. K.; Elings, V. B.; Marti, O.; Bracker, C. E. Science 1988, 242, 209.
6. Albrecht, T. R.; Quate, C. F. J Vac Sci Technol A 1988, 6, 271.
7. Bowen, W. R.; Mohammad, A. W.; Hilal, N. J Memb Sci 1997, 126, 91.
8. Bowen, W. R.; Hilal, N.; Jain, M.; Lovitt, R. W.; Mohammad, A. W.; Sharif, A. O.; Williams, P. M.; Wright, C. J. In Comprehensive Chemical Kinetics, Vol. 37, Application of Kinetic Modelling; Compton, R. G.; Hancock, G.; Eds.; Elsevier: New York, 1999; 524.
9. Bowen, W. R.; Hilal, N.; Lovitt, R. W.; Wright, C. J. J Membr Sci 1998, 139, 269.
10. Mohammad, A. W.; Nora'aini Ali; Nidal Hilal, Separ Sci Technol 2003, 38(6), 1307.
11. Wang, X. L.; Tsuru, T.; Togoh, M.; Nakao, S.; Kimura, S. J Membr Sci 1997, 135, 19.
12. Schaep, J.; Vandecasteele, C.; J Membr Sci 2001, 188, 129.
13. Schaep, J.; Vandecasteele, C.; Mohammad, A. W.; Bowen, W. R. Separ Purif Technol 2001, 22–23(1–3), 169.
14. Mohammad, A. W. Separ Sci Technol 2002, 37(5), 1009.
15. Bowen, W. R.; Mohammad, A. W. Trans IChE, 1998, 76A, 885.
16. Bowen, W. R.; Mohammad, A. W. Desalination 1998, 117, 257.
17. Mohammad, A. W.; Hilal, N.; Nizam, M.; Abu Seman, M. N. Desalination 2003, 158, 73.
18. Sarid, D. Scanning Force Microscopy; Oxford University Press: Oxford, 1994.
19. Matsuura, T. Desalination 2001, 134, 47.
20. Ji, J.; Mehta, M. J Membr Sci 2001, 192, 41.
21. Bowen, W. R.; Mohammad, A. W. AIChE J 1998, 44, 1799.